J. Fluid Mech. (2008), *vol.* 606, *pp.* 369–397.
doi:10.1017/S0022112008001924 Printed in the United Kingdom

Simulation of flow around a row of square cylinders

SHASHI RANJAN KUMAR, ATUL SHARMA AND AMIT AGRAWAL

Department of Mechanical Engineering, Indian Institute of Technology – Bombay, Powai, Mumbai, 400076, India

(Received 18 March 2007 and in revised form 19 March 2008)

In this paper, the low-Reynolds number ($Re = 80$) flow around a row of nine square cylinders placed normal to the oncoming flow is investigated using the lattice-Boltzmann method. The effects of the cylinder spacing on the flow are studied for spacing to diameter ratios of 0.3 to 12. No significant interaction between the wakes is observed with spacings greater than six times the diameter. At smaller spacings, the flow regimes as revealed by vorticity field and drag coefficient signal are: synchronized, quasi-periodic and chaotic. These regimes are shown to result from the interaction between primary (vortex shedding) and secondary (cylinder interaction) frequencies; the strength of the latter frequency in turn depends on the cylinder spacing. The secondary frequency is also related to transition between narrow and wide wakes behind a cylinder.

The mean drag coefficient and Strouhal number are found to increase rapidly with a decrease in spacing; correlations of these parameters with spacing are proposed. The Strouhal number based on gap velocity becomes approximately constant for a large range of spacings, highlighting the significance of gap velocity for this class of flows. It is also possible to analyse the vortex pattern in the synchronized and quasi-periodic regimes with the help of vorticity dynamics. These results, most of which have been obtained for the first time, are of fundamental significance.

1. Introduction

The flow downstream of a row of cylinders placed normal to the flow has many practical engineering applications. A row of cylinders is often used to screen strong and sudden winds in order to change them to weak and gentle ones (Mizushima & Takemoto 1996). Cascades of cylinders, with a narrow spacing between the cylinders, are often used in wind tunnels to obtain a uniform velocity distribution; but the velocity distribution is prevented from becoming uniform when cylinders are put too close to each other (Bradshaw 1965). The flow past a row of cylinders is of interest in situations such as turning vanes in duct elbows, multi-slotted airfoils, and flow around closely spaced electrical power poles (Cheng & Moretti 1988). The flow around multiple cylinders is a spatially developing flow problem, where several rich phenomena are observed.

In this paper, we numerically study flow around a row of square cylinders placed side-by-side, at low Reynolds number. Square cylinders were chosen for the present study because they can be described on a Cartesian grid with a higher accuracy as compared to circular cylinders. The cylinders are assumed to be of equal size (d) and the distance between two consecutive cylinders (s) is the same. For a row of cylinders,

the important parameters are non-dimensional spacing, s/d and Reynolds number, Re ($=U_0 d/\nu$ where U_0 is the uniform inlet velocity and ν is the kinematic viscosity of the fluid). A study with a row of square cylinders at low Reynolds numbers does not seem to have been undertaken before. However, some studies on two to five cylinders and a row of nine or more circular cylinders at high Reynolds numbers are available. Some difference in results between circular and square cylinders can be expected because unlike the circular cylinder, the square cylinders tend to fix the separation point, causing differences in the critical regimes. The separation mechanism and the consequent dependence of the shedding frequency and the aerodynamic forces as a function of Reynolds number, also differs significantly for the two geometries. In the following sections, we present a brief summary of these earlier works. The relevant studies for two (and more) cylinders are used throughout the paper for comparison with the simulation results.

1.1. *Literature survey for two-five cylinders*

Bearman & Wadcock (1973) studied quasi-stable and flopping for two circular cylinders as a function of cylinder spacings, at a Reynolds number of 2.5×10^4. Quasi-stable behaviour is the behaviour observed downstream of the cylinders with different values of drag coefficient C_d. A large-amplitude flow perturbation can cause the C_d value to change, but the C_d remains at the new value until another large perturbation is applied. On the other hand, flopping is the behaviour where C_d alternates over time between relatively high and low values, even when no perturbation is applied to the flow field. Bearman & Wadcock (1973) showed that when $s/d \geqslant 4.0$, the cylinder wakes do not interact until after a significant distance downstream. The cylinders must be nearly touching for a single wake to form. Kim & Durbin (1988) worked with $s/d = 0.75$ and Reynolds number between 2200 and 6200. Only flopping was observed in their experiments. Le Gal *et al.* (1990) performed experiments using two cylinders with $s/d \leqslant 6.5$ and $Re = 110$ and found wake interaction up to a separation ratio of about 4.5. Probably because of the low Reynolds number, flopping was difficult to observe in their study. However, they did observe quasi-stable behaviour and performed a flow-visualization study which was in agreement with the large-wake and small-wake model presented later. Sumner *et al.* (1999) used particle image velocimetry to examine the vorticity field behind the cylinders. Several numerical studies have also been carried out for circular cylinders (Slaouti & Stansby 1992; Farrant, Tan & Price 2001; Meneghini *et al.* 2001; Kang 2003). Most of these studies which present the lift and drag coefficients as a function of time, were undertaken either to verify the various numerical schemes that were used, or to extend the available experimental results.

Zhou *et al.* (2000) presented a detailed phase-average-based analysis of hot-wire data in an effort to educe the vortices in the flow for two and three cylinders in the flow. They have also systematically analysed two of the ensuing flow regimes. Guillaume & LaRue (1999) investigated the different flow regimes for different spacings for two, three and four cylinders placed normal to the flow. They report the presence of multiple peaks in the power spectra corresponding to different values of the Strouhal number. They also observed anti-phase flopping behind two-cylinder-row and quasi-stable behaviour behind three and four cylinders.

Ishigai & Nishikawa (1975) experimentally investigated the flow downstream of five side-by-side circular cylinders for $Re = 4000$–$33\,000$, along with other configurations not of interest here. They used the schlieren technique with special attention to dependence of the vortex-formation region and the Coanda effect on the gap flow.

The Strouhal number almost doubled when the spacing was reduced from $s/d = 1.5$ to 0.2.

All the above investigations were for circular cylinders. Kolar, Lyn & Rodi (1997) performed measurements on a pair of square cylinders using two-component laser-Doppler velocimetry at $\mathrm{Re} = 23\,100$ and $s/d = 2$. They performed phase-averaging and examined the strengths of the vortices both near the gap and in the outer shear layers. Valencia & Cid (2002) and Agrawal, Djenidi & Antonia (2006) performed a numerical study of the flow around a pair of square cylinders. Agrawal *et al.* (2006) showed the presence of synchronized and chaotic regimes with square cylinders at $Re = 73$, in agreement with the well-known results for circular cylinders. Their study shows in-phase shedding to be the predominant mode in the synchronized regime, whereas application of the linear stochastic estimate technique showed that both in-phase and anti-phase configurations occur with almost equal probabilities in the flip-flop regime.

1.2. *Literature survey for a row of cylinders*

Cheng & Moretti (1988) presented flow-visualization images and velocity measurements of the flow field downstream of a row of nine tubes at $s/d = 0.3$ and $Re = 2500$. Bradshaw (1965) performed experiments on a row of nine circular cylinders to obtain the stability limit for the merging of vortices at a Reynolds number of 1500. Chauve & Le Gal (1992) performed flow visualization on a row of 16 cylinders at $s/d = 3$ and $Re = 80$. They report that at certain instants, certains wakes stop oscillating (shedding vortices); these events appear erratically in time and can affect any wake. Analysis of the recorded images revealed spatio-temporal chaos, which was consistent with their simulations of the generalized Ginzburg–Landau equation. The above analysis was extended to other spacings ($s/d = 0.5$ and 2) by Le Gal *et al.* (1996).

Mizushima & Takemoto (1996) performed flow visualization of the pattern downstream of a row of square cylinders. For $1.2 \leqslant s/d \leqslant 2.6$ and $80 \leqslant Re \leqslant 320$, their result shows that at specific Reynolds number and s/d combinations, both flopping and bi-stable flip-flop behaviour can exist downstream of the cylinders. Mizushima & Akinaga (2003) investigated interactions of wakes in flow past a row of square and circular bars, placed across uniform flow by numerical simulations and experiments. Their result shows that at $s/d = 1.0$, in-phase vortex shedding occurs between cylinders whereas at $s/d = 3.0$, anti-phase shedding was observed.

The literature survey shows that although there are a number of studies for single and a pair of cylinders, there is limited information for flow around a larger number of cylinders. It is also noted that there is limited quantitative information on a row of cylinders in the available papers, and no sincere effort to document and understand the different flow regimes that can exist has been made. An infinite row of cylinders is the other extreme of a single-cylinder case, and the results are expected to be of fundamental value, besides being important for several applications mentioned above. The present work attempts to fill some of these voids. Specifically, we focus on the low-Reynolds-number end for a row of square cylinders. Simulations are performed for the entire range of spacings ($s/d = 0.3$–12), at a fixed Reynolds number of 80. The resulting vorticity fields along with the time series for drag and lift coefficients are examined, with the aim of defining and explaining the resulting flow patterns. We also explain the origin of a new (cylinder interaction) frequency, which is clearly seen from the data and substantially affects the behaviour.

2. Computational details

A brief description of computational technique and boundary conditions employed, along with validation of the code and data-reduction techniques is provided in this section. Although the lattice-Boltzmann method (LBM) has been used in the present study, an alternative computational technique (such as finite-volume method) could have been used. Some advantages of using LBM as compared to conventional techniques are ease of placing cylinders in the flow and parallelization of the code. A parallel code has, however, not been used in the present computations.

2.1. *Lattice Boltzmann method*

In the LBM approach, we solve the kinetic equation for the particle velocity distribution function f. A D2Q9 scheme (where D refers to space dimensions, and Q to the number of particles at a computational node) is adopted for this work. Here, each node comprises eight moving particles and a rest particle. The density evolution equation is given by

$$f_i(\boldsymbol{x}+\boldsymbol{e}_i, t+1) = f_i(\boldsymbol{x}, t) - \frac{f_i(\boldsymbol{x}, t) - f_i^{eq}(\boldsymbol{x}, t)}{\tau}, \tag{1}$$

where f_i is the instantaneous particle density at a link, f_i^{eq} is the corresponding equilibrium density, $\boldsymbol{x}$ is the spatial position vector, $\boldsymbol{e}_i$ are the direction vectors, t is time, and τ is the relaxation time. The equilibrium density function is computed as

$$f_i^{eq} = \rho w_i \left(1 + 3(\boldsymbol{e}_i \cdot \boldsymbol{u}) + \tfrac{9}{2}(\boldsymbol{e}_i \cdot \boldsymbol{u})^2 - \tfrac{3}{2}u^2\right), \tag{2}$$

where $\boldsymbol{u}$ is the instantaneous velocity at the node, ρ is the fluid density, and w_i are the corresponding weights ($w_i = 4/9$ for rest particle, $1/9$ for axis particles and $1/36$ for diagonal particles). The relaxation time is related to the kinematic viscosity of the fluid via the relation $\nu = (2\tau - 1)/6$.

Equation (1) is solved through the two steps of collision (which uses a BGK collision operator; Chen & Doolen 1998) and propagation, i.e. (3) and (4) given below. During the collision step, the particles readjust their states while the overall mass and momentum at the computational node is conserved. In the subsequent step (propagation), the particles move to the nearest neighbours along their respective velocity directions. Mathematically, these steps can be expressed as (collision)

$$f_i^{new}(\boldsymbol{x}, t) = f_i(\boldsymbol{x}, t) - \frac{f_i(\boldsymbol{x}, t) - f_i^{eq}(\boldsymbol{x}, t)}{\tau}, \tag{3}$$

where f_i^{new} is an intermediate function, and (propagation)

$$f_i(\boldsymbol{x}+\boldsymbol{e}_i, t+1) = f_i^{new}(\boldsymbol{x}, t). \tag{4}$$

The boundary conditions are applied after the propagation step equation (4), and the entire process is solved iteratively.

The density (ρ), velocity ($\boldsymbol{u}$) and pressure (p) at a node are calculated from the following equations:

$$\rho = \sum_i f_i, \quad \rho\boldsymbol{u} = \sum_i f_i \boldsymbol{e}_i, \quad p = \rho c^2, \tag{5}$$

where c is the speed of sound ($= 1/\sqrt{3}$ in our scheme). It has been shown mathematically that the solution of (1) using the above two steps is equivalent to solving the Navier–Stokes equations provided that the underlying lattice has a sufficient amount of symmetry (Frisch, Hasslacher Pomeau 1986; Succi 2001).

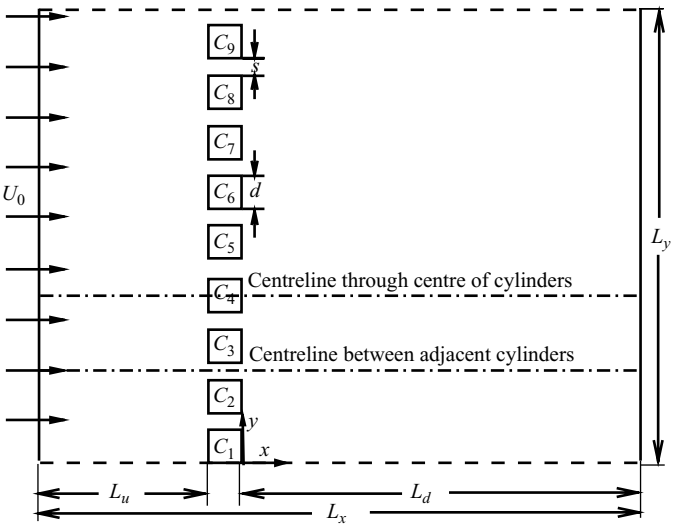

FIGURE 1. The computational domain. The size of the computational domain (L_x, L_y) is $(27d,9(d+s))$. The nine cylinders present have been marked as C_1 to C_9, starting from the bottom of the computational domain. Note that the origin of the coordinate system has been fixed at the lower-downstream vertex of the bottom-most cylinder.

2.2. *Computational domain, boundary and initial conditions*

The flow configuration is shown in figure 1. Nine fixed two-dimensional square cylinders with side d, which is also the characteristic length scale, are exposed to a constant and uniform velocity U_0. The length of the computational domain is taken to be $L_x = L_u + d + L_d$, where L_u is the upstream length and L_d the downstream length from the origin. Mizushima & Takemoto (1996) have taken $L_u = 4.5d$ and $L_d = 15.5d$ in their numerical simulations for a row of square cylinders. The dimensions of the computational domain were checked by them by requiring that the length of the twin vortices attached to the square bars does not change significantly even if the dimensions are increased. Our preliminary tests with $L_u = 7d$ and $L_d = 19d$ confirmed that the cylinders are properly placed with respect to the edges of the computational domain. Therefore, these latter values are employed in the simulations for most of the cases presented here. The number of points along the lateral direction is L_y $(= 9(d+s))$. Note that the underlying grid structure is uniform and square. It is important to realize that nine cylinders are actually present in the computational domain, unlike some previous studies where the flow around a single cylinder was computed, and by employing either symmetric or periodic boundary condition the results were extended to other cylinders.

A periodic boundary condition has been applied on the lateral sides of the computational domain for extending the results to an infinite number of cylinders (figure 1). The popular approach of using the bounce-back scheme has been employed to simulate the no-slip condition at the fluid–solid interfaces (see Agrawal & Agrawal 2006 for details about its implementation). A uniform velocity with negligible compressibility effects $(U_0/c = 0.0866)$ was prescribed at the inlet. A convective boundary condition has been used at the outlet, which allows an unconstrained movement of the fluid away from the computational domain. The simulation starts with the fluid initially at rest.

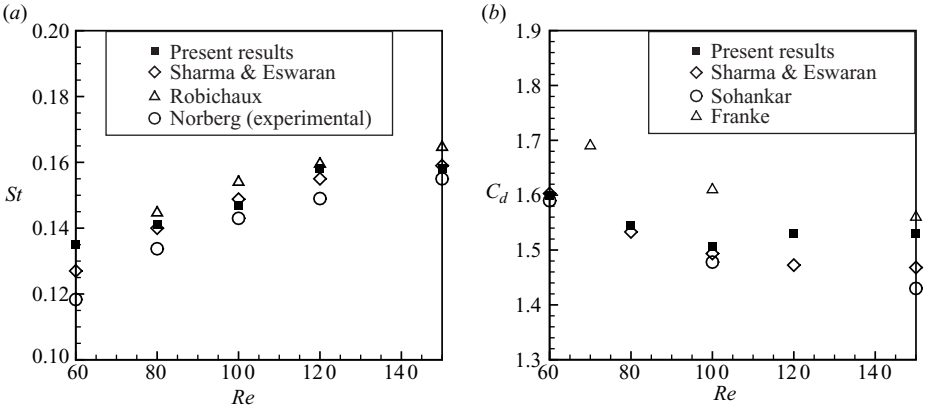

FIGURE 2. Comparison of (*a*) Strouhal number, and (*b*) coefficient of drag as a function of Reynolds number for a single cylinder, against available experimental and numerical data. The experimental data of Norberg have been taken from Sohankar, Norberg & Davidson (1997).

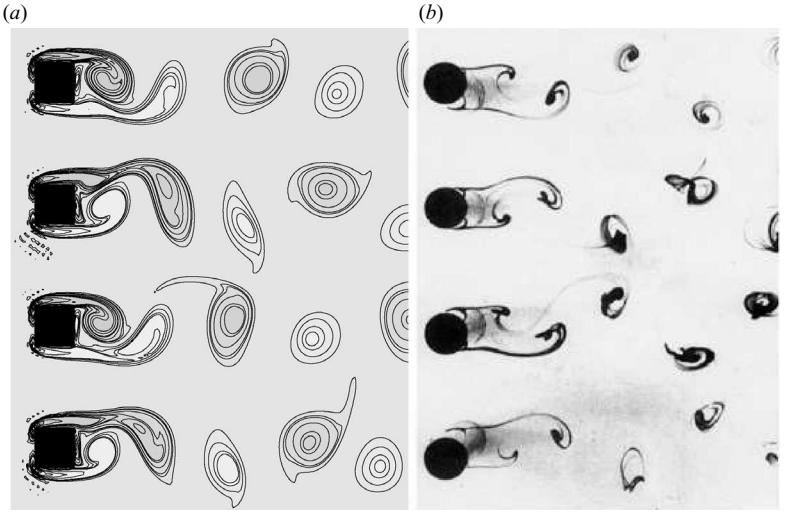

FIGURE 3. Comparison of vortex shedding from a row of cylinders ($s/d = 2.0$ and $Re = 200$). (*a*) Present computations, and (*b*) experiments of Kobayashi (1984) (taken from Mizushima & Akinaga 2003).

2.3. *Validation of the code and adequacy of the grid*

This code for the large-cylinder case is essentially an extension of two-cylinder code used in Agrawal *et al.* (2006). The code with minimal modifications has also been used elsewhere (e.g. Burattini *et al.* 2006). The code was validated by comparing results for a single square cylinder against published data, as mentioned in Agrawal *et al.* (2006). Additional validation for a single square cylinder in a uniform flow is provided in figure 2. Figure 3 compares the flow pattern for a row of cylinders as computed from the present code against the experimental result of Kobayashi (1984). Although the geometry of the cylinders is different (because of the paucity of results for square

s/d	d	$L_x \times L_y$
0.3	50	1350×585
0.4	40	1080×504
1.0	20	540×360
1.8	10	270×252
2.0	20	540×540
2.2	20	540×576
2.5	10	270×315
3.0	16	432×576
4.0	16	432×720
5.0	10	270×540
6.0	10	270×630
8.0	10	270×810
10.0	10	270×990
12.0	10	270×1170

TABLE 1. The number of points representing one cylinder dimension and the total computational domain employed at different spacings.

s/d	C_d at $d = 10$	C_d at higher resolution
1.0	6.147 (5.2 %)	6.485 at $d = 20$
2.0	3.287 (4.3 %)	3.152 at $d = 20$
2.2	3.023 (5.6 %)	2.863 at $d = 20$
4.0	2.073 (7.4 %)	1.931 at $d = 16$

TABLE 2. Effect of spatial resolution on the mean coefficient of drag (C_d) at $Re = 80$. The figure in parentheses shows the difference between values at lower and higher resolution grid (in percentage), taking the higher grid-point value as the base. Note that for all these cases the higher of the two resolutions is employed in the computations.

cylinders at low Reynolds numbers), the result agrees reasonably well. These results establish confidence in predictions from the present code.

The grid-size and solution employed in the simulations have been tabulated for different cases in table 1. The resolution is chosen such that both flow around the cylinder and in the gap are best resolved, keeping the constraints of computational resources and simulations for long time in mind. The spatial adequacy was tested by varying the number of grid points representing a cylinder and comparing values of C_d for different resolutions (see table 2). The difference is within 7 %, implying that the computations on the higher resolution are grid independent with respect to the chosen parameter for all spacings.

Earlier studies (e.g. Saha, Muralidhar & Biswas 2000; Ravoux, Nadim & Haj-Hariri 2003) show that satisfactory results have been achieved with a comparable spatial resolution. The results of Breuer *et al.* (2000) indicated that a higher resolution is required only at larger Reynolds numbers. The low Reynolds number ($Re = 80$) employed in the simulations further ensures that the flow is two-dimensional (as shown by Saha, Biswas & Muralidhar 2003, three-dimensional effects become important only around $Re = 175$ for a single square cylinder; Chauve & Le Gal 1992 also chose $Re = 80$ in their experiments for the same reason). However, no explicit test to check for spanwise flow homogeneity was performed.

2.4. *Data reduction*

From the primary code, results are obtained for velocity and pressure field for the entire computational domain. Additional quantities such as drag and lift coefficients, vorticity and Strouhal number are computed from velocity and pressure fields for further analysis. The lift (C_l) and drag (C_d) coefficients are calculated in the usual manner:

$$C_l = \frac{F_l}{\frac{1}{2}A\rho U_0^2}, \quad C_d = \frac{F_d}{\frac{1}{2}A\rho U_0^2}, \tag{6}$$

where F_l and F_d are the lift and drag forces, respectively, and A is the frontal area. Note that these forces comprise both pressure force and viscous drag components. (See Kumar 2006, for details about computation of these forces).

Flow patterns obtained in different regimes have been analysed on the basis of vortex interaction (Kundu 1990). The first step was to compute the vorticity field; the vortex centre is found next, and subsequently its shape, strength (or circulation, Γ) and rotational sense are calculated. Then assuming vortices to be two-dimensional (perpendicular to the paper), the effect of other vortices on the movement of a given vortex is found. The velocity induced owing to a vortex $\boldsymbol{v}$ at a distance r from the vortex centre is (Kundu 1990):

$$\boldsymbol{v} = \frac{\Gamma}{2\pi r}\boldsymbol{e}_\theta, \tag{7}$$

where, Γ is calculated using (8) below, and $\boldsymbol{e}_\theta$ is a unit vector. The direction of the induced velocity ($\boldsymbol{e}_\theta$) is perpendicular to the line joining the vortex centre to the point of interest, and depends on the rotational sense of the vortex.

The centre of a vortex in the flow is located by finding the local maxima in the vorticity field. The maxima is identified by comparing the vorticity at every point to its 24 neighbours. Some noise (spurious centres) may, however, remain; most of these are eliminated by thresholding (the vortices with strengths less than half of the mean strength of all detected vortices are removed). Benchmarking of centre identification is done by matching the vortex centres to centres found in streamlines and velocity vector plots by overlapping the three (Kumar 2006). Vortex shape is computed by finding the region around the identified vortex-centre where vorticity first becomes less than 5 % of the vorticity at the centre of that vortex. The basis of choosing 5 % as the cutoff vorticity value is related to the strength of the vortex. The vortex strength is calculated as

$$\Gamma = \oint_A \boldsymbol{\omega}\cdot \mathrm{d}\boldsymbol{A}, \tag{8}$$

where $\boldsymbol{\omega}$ is vorticity, and $\boldsymbol{A}$ is the area with vorticity greater than or equal to 0.05 times the peak vorticity. Integration is also done over the area with vorticity greater than or equal to 0.10 times the peak vorticity; the difference in the resultant strength is less than 3 % with respect to the 0.05 criteria. Hence, it was concluded that including regions with greater than or equal to 0.05 times peak vorticity for the strength calculation is sufficient to capture the entire vortex. The educed shape is compared with vorticity contours to establish confidence in the computed vortex shape. Figure 4 shows that the present algorithm faithfully reproduces the shape of the vortices.

2.5. *Determination of the minimum number of cylinders*

In this section, we examine the mininum number of cylinders required to simulate a row. Preliminary computations are done for a given spacing ($s/d = 4.0$) and Reynolds number ($Re = 80$), while the number of cylinders in the computational domain is

n_{cyl}	C_d
4	1.705
7	1.915
8	1.910
9	1.931
10	1.916

TABLE 3. Comparison of mean coefficient of drag from row of four, seven, eight, nine and ten cylinders ($s/d = 4.0$, $Re = 80$). n_{cyl} stands for number of cylinders present in the computational domain.

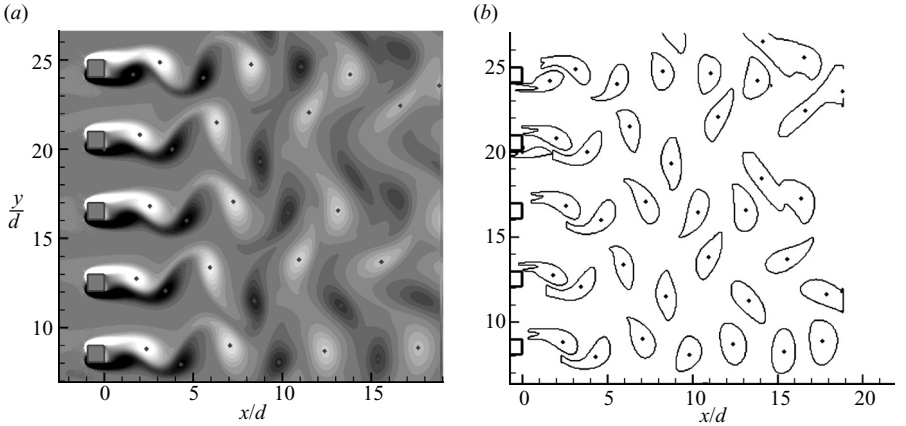

FIGURE 4. Verification of the vortex centre and shape as determined by the detection algorithm ($s/d = 3.0$, $Re = 80$). (*a*) The vorticity contour plot overlapped with the vortex-centres detected, and (*b*) the vortex shape plot as determined by our algorithm.

varied (4, 7, 8, 9 and 10). Table 3 shows that the mean drag coefficient is almost invariant when 7 or more cylinders are present in the flow. Because the same results are obtained with 7 to 10 cylinders, the number of cylinders can be arbitrarily chosen and is fixed to 9 for further computations. This number appears large enough to simulate a row of infinite cylinders.

3. Flow patterns and time-signal analysis

Simulations are first done at a spacing of $s/d = 12$ and the spacing is reduced successively. The results for $s/d = 12$, 10 and 8 are similar and only a few notable observations are made. For these spacings, almost no interaction occurs between the flow behind adjoining cylinders. This is deduced, for example, by examining the width of the wake and mean and r.m.s. velocity fields (not shown). However, the only way to confirm it is by starting the simulation with different phase lags in vortex shedding from the cylinders; for no interaction, the phase lag would remain invariant with time (P. Burattini, personal communication, 2004). However, this was not done because it is tedious and the same result can be obtained by examining the mean C_d and St, as discussed in § 4. Because of insignificant interaction between the wakes, little investigation is done at those separation ratios.

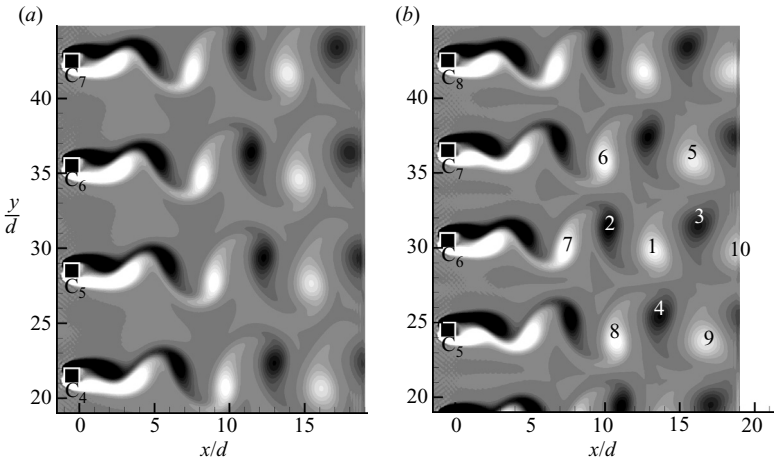

FIGURE 5. Vortex shedding from cylinders in the synchronized regime for (*a*) $s/d = 6.0$, and (*b*) $s/d = 5.0$ ($Re = 80$). The location of the cylinders is marked by a black square with a white outline.

When $s/d \leqslant 6.0$, the wakes behind the cylinders interact in a complicated manner, resulting in a variety of flow patterns. We follow the flow pattern over several vortex-shedding cycles before making conclusions about them. All the results presented below are after the initial (numerical) transients have died out.

3.1. *Synchronized flow* ($4.0 < s/d \leqslant 6.0$)

For configurations with $s/d = 5.0$, 6.0 vortices shed from any cylinder have a constant frequency and a definite phase relationship with vortices shedding from other cylinders. For $s/d = 6.0$ (figure 5*a*), shedding is almost in-phase because vortices of the same colour corresponding to shedding from consecutive cylinders are at approximately the same streamwise location; a closer look reveals a phase lag of 30°. In this case, the vortices remain distinct throughout the computational domain, unlike some other regimes presented later. This is probably because of weak interactions owing to large spacing between the cylinders.

For $s/d = 5.0$, the vortices are shed roughly in anti-phase mode from consecutive cylinders because, black (white) vortices shedding from top (bottom) half of cylinder and white (black) vortices shedding from bottom (top) half of cylinder just above (below) previous cylinder are approximately at the same x/d (figure 5*b*). Because the above-mentioned vortices are not at exactly the same x/d, the phase lag differs from 180°, as summarized in § 4. For the anti-phase mode, similar to the in-phase mode, there is little movement of fluid across the gap centreline, and the wakes develop without significant lateral spread. Similar flow configurations have been reported by Williamson (1985) for two circular cylinders at $s/d = 3$ and $Re = 100$. Williamson further noted that the vortex configuration is 'stable', i.e. the configuration keeps its form for a large downstream distance. (While comparing with the two-cylinder result, we can see that a given flow regime appears at a larger spacing with a row of cylinders.)

The observations about in-phase and anti-phase are supported by the time series for lift coefficient C_l of any two adjoining cylinders. Figure 6 for $s/d = 5.0$ shows that both lift and drag coefficients are sinusoidal in shape. Whereas the amplitude of C_l is constant (with a zero mean), the amplitude of C_d alternates between 0.02 and 0.03

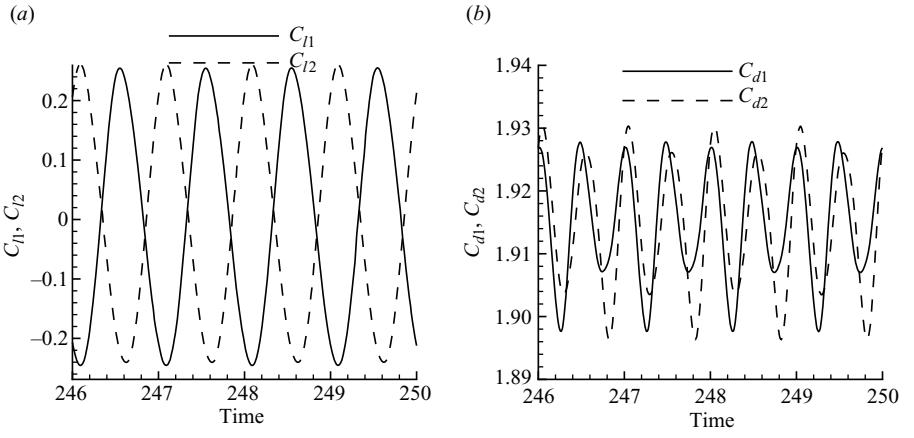

FIGURE 6. Signal of lift and drag coefficients for $s/d = 5.0$, $Re = 80$: (*a*) C_{l1}, C_{l2} versus time, and (*b*) C_{d1}, C_{d2} versus time. Note that the subscripts '1' and '2' refer to the cylinder number, and the time on the abscissa has been normalized by the corresponding vortex shedding period.

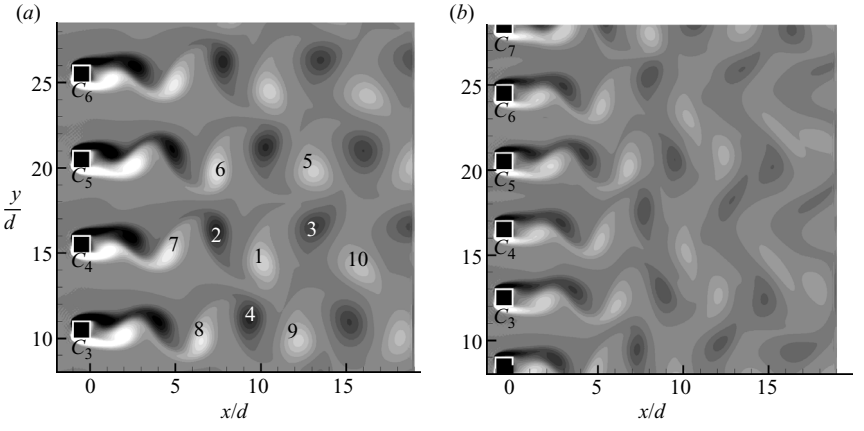

FIGURE 7. Vortex shedding from cylinders for (*a*) $s/d = 4.0$ and (*b*) $s/d = 3.0$ ($Re = 80$). The location of the cylinders is marked by a black square with a white outline.

for successive cycles with 1.920 as the mean. The frequency of C_l is half of C_d which is consistent with observations in a single cylinder, and the phase difference between C_{l1} and C_{l2} is about 200°. The drag coefficents are approximately in-phase, which is consistent with the observation that the same event which leads to an extremum in lift is responsible for a maximum in drag.

3.2. *Quasi-periodic flow-I* ($3.0 \leqslant s/d \leqslant 4.0$)

For both $s/d = 4.0$ and 3.0, the vortices are again clearly apparent (figure 7); however, there is some evidence of merging of vortices in $s/d = 3.0$ at further downstream locations ($x/d \geqslant 7$). The vortex shedding from a cylinder appears to have a definite phase relationship with shedding from any other cylinder. However, a closer look reveals that, the time period of consecutive sheddings from a cylinder is not constant, as discussed below.

The time signal for lift and drag coefficients between two consecutive cylinders have been plotted in figure 8. The C_d signal (figure 8*b*, *d*) does not resemble the simple

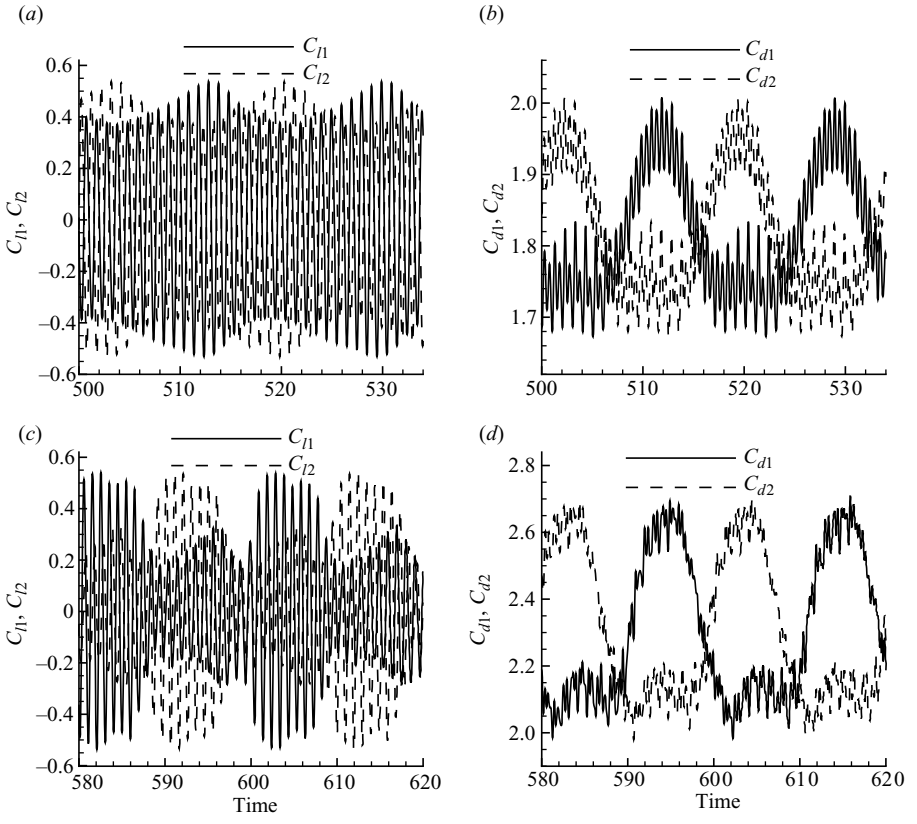

FIGURE 8. Signal of lift and drag coefficients for $s/d = 4.0$, 3.0 and $Re = 80$. (*a*) C_{l1}, C_{l2} versus time for $s/d = 4.0$, (*b*) C_{d1}, C_{d2} versus time for $s/d = 4.0$, (*c*) C_{l1}, C_{l2} versus time for $s/d = 3.0$, and (*d*) C_{d1}, C_{d2} versus time for $s/d = 3.0$. Note that the time on the abscissa has been normalized by the corresponding average shedding period.

sinusoidal variation of the C_l or C_d signal for a single cylinder, or of figure 6, rather, it shows a modulated sine with a flat lower half. The modulation (secondary) frequency spans over 17 and 21 vortex-shedding (primary) cycles, respectively. Similarly, there is a modulation frequency in the C_l signal (figure 8*a*, *c*) These two frequencies lead to the presence of multiple peaks in the power spectra of the drag coefficient signal, corresponding to different values of Strouhal number (figure 9 for $s/d = 4.0$).

Based on the periodicity of lift coefficient signals, the peak at a Strouhal number of 0.175 is associated with a shedding frequency at $s/d = 4.0$. Since the wakes formed behind the cylinder are symmetric about the cylinder centreline, the periodicity of the drag coefficients is half of the shedding period, and a peak of larger magnitude is observed at $St = 0.35$. The peaks (not seen) at a Strouhal number of 0.53, 0.7 and 0.88 are believed to be harmonics of the peak at 0.175 (being three, four and five times this number). The peak at a Strouhal number of 0.01 in the power spectrum corresponds to secondary frequency, i.e. the secondary period is about 17 times the shedding period. Again, the peaks at Strouhal numbers of 0.02 and 0.03 are harmonics of the secondary frequency. The remaining peaks are linear combinations of primary and secondary frequencies.

s/d	Number of time iterations for one primary period
4.0	1840, 1840, 1820, 1810, 1790, 1800, 1790, 1810, 1810, 1830, 1830, 1840, 1850, 1860, 1860, 1860, 1860
3.0	1640, 1840, 1700, 1590, 1610, 1600, 1600, 1600, 1610, 1580, 1610, 1610, 1620, 1640, 1730, 1690, 1700, 1670, 1690, 1730, 1720

TABLE 4. Sequence of primary periods encompassed in a secondary cycle for different spacings. (Note that 1830 time iterations correspond to a Strouhal number of 0.175.)

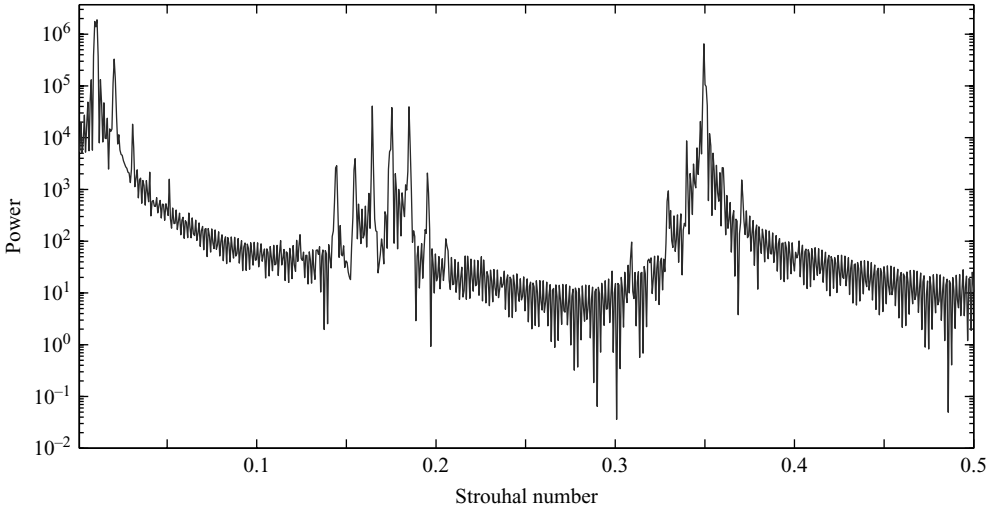

FIGURE 9. Power spectra of drag coefficient signal, for a nine-cylinder row at $s/d = 4.0$ and $Re = 80$. Power is in arbitrary units.

An examination of the time series for C_d reveals that the secondary time period is constant (with period = 31 100 time iterations) for each cylinder. Within one secondary period, the primary periods have slightly different values (up to 4 % variation for $s/d = 4.0$, see table 4); however, it was verified that every secondary period for each cylinder has the same sequence of primary cycles. The sequence of primary periods is presented in table 4. For $s/d = 3.0$, the secondary time period is again constant across secondary cycles and for each cylinder. Here, each secondary cycle comprises 21 primary cycles with a total of 34 780 time iterations. The sequence of primary periods is also presented in table 4. Note that within one secondary period, the primary period has different values and the variation is more here (10 %) than for $s/d = 4.0$. The number of primary cycles in a secondary cycle is therefore dependant on s/d; there is, however, no reason to believe that this number should always be an integer. It can be speculated that transition to the quasi-periodic-II regime occurs when an irrational number of primary cycles are encompassed in a secondary cycle.

Chauve & Le Gal (1992) mentions that a difference of about 15 % can exist in the frequencies of a row of circular cylinders at $s/d = 3$, $Re = 80$. They also found a modulation in the amplitude with a period larger than their sample size (which was relatively small) and a phase shift of 180°. The results from the present simulations compare favourably with their findings.

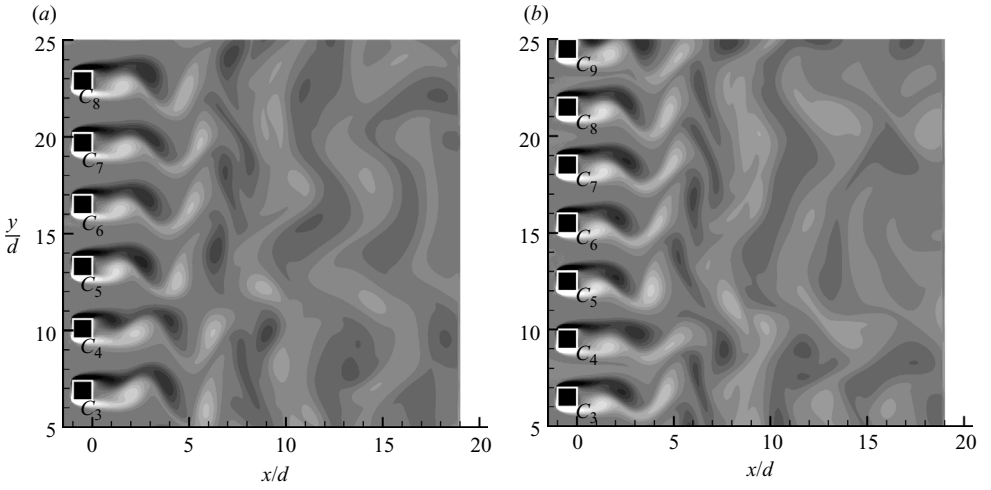

FIGURE 10. Vortex shedding from cylinders for (*a*) $s/d = 2.2$, and (*b*) $s/d = 2.0$ ($Re = 80$). The location of the cylinders is marked by a black square with a white outline.

3.3. *Quasi-periodic flow-II* ($1.0 < s/d < 3.0$)

Figure 10 with $s/d = 2.2$ and 2.0 reveals that while the vortices immediately downstream of the cylinders are clearly apparent, those further downstream have merged. The downstream distance around which this merging happens ($x/d \approx 5$) is smaller than in the previous regime; the vortices also tend to lose their identities completely upon merging in the present regime unlike the quasi-periodic-I regime. The instantaneous vorticity contours further reveal that the shedding is neither in in-phase nor in anti-phase. For example, in figure 10(*a*) cylinders C_3 and C_4, and cylinders C_5 and C_6 are shedding in in-phase while cylinders C_4 and C_5 are shedding in anti-phase. However, the time series for lift and drag coefficients does not reveal a predominance of either of these two modes (figure 11). A linear stochastic estimate for two cylinders with $s/d = 0.7$ and $Re = 73$ revealed the presence of both in-phase and anti-phase shedding (Agrawal *et al.* 2006); however, it is difficult to discern these underlying modes without the use of special data-processing techniques.

The drag coefficient shows a more chaotic behaviour than the signal for lift coefficient (figure 11). This shows that the dynamics of lift and drag coefficients become decoupled for a square cylinder. Further, the period of vortex shedding from a given cylinder as deduced from the C_d signal, is not constant. With $s/d = 4.0$ (figure 8*b*), the variations in C_d due to secondary and primary cycles are 0.33 and between 0.04 and 0.16, respectively. Similarly in the C_d signal for $s/d = 2.2$ (figure 11*b*), the large-scale and small-scale variations are 0.80 and 0.02–0.44, respectively, which can be attributed to secondary and primary frequencies respectively. The corresponding numbers for $s/d = 2.0$ (Fig. 11*d*) are 0.96 and 0.01–0.39. Note the increase in amplitude of secondary frequency with a decrease in spacing. However, unlike the previous regime, in the present regime, the period of secondary cycles is not constant. These series, however, suggest that the consecutive cylinders are roughly in anti-phase with respect to the secondary frequency, meaning that (as discussed later), when a wide wake is formed behind one cylinder, a narrow wake is formed behind the adjoining cylinders, and vice versa.

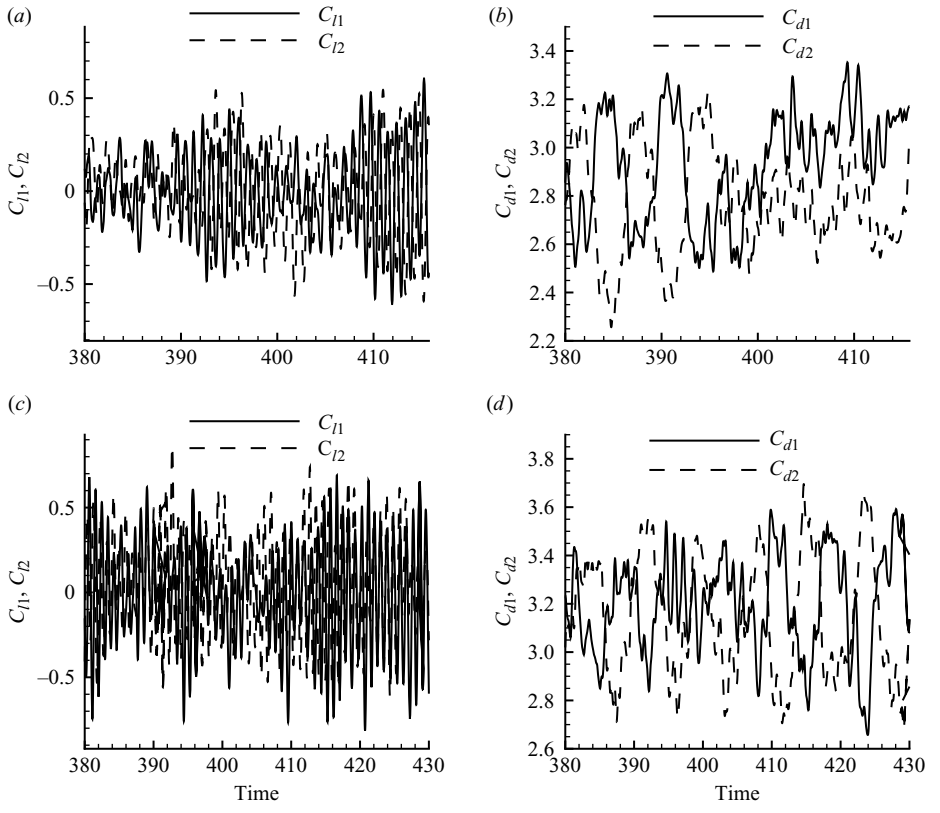

FIGURE 11. (*a*) Signal of lift and drag coefficients for $s/d = 2.2$, 2.0 and $Re = 80$. C_{l1}, C_{l2} versus time for $s/d = 2.2$, (*b*) C_{d1}, C_{d2} versus time for $s/d = 2.2$, (*c*) C_{l1}, C_{l2} versus time for $s/d = 2.0$, and (*d*) C_{d1}, C_{d2} versus time for $s/d = 2.0$. Note that the time on the abscissa has been normalized by the corresponding average shedding period.

Because it is difficult to obtain the Strouhal number from the curves presented above, a spectral analysis is performed to obtain this information. The small peak in the power spectra of time series of drag coefficient at $St = 0.012$ for $s/d = 2.0$ (figure 12) is believed to correspond to secondary frequency. A Strouhal number of 0.22 corresponds to the primary shedding frequency, whereas the peaks at Strouhal numbers of 0.44 and 0.88 are its harmonics.

Kim & Durbin (1988) presented the first statistical analysis of the time interval for which the C_p value remains relatively high and the time for which it is relatively low ($s/d = 0.75$). They showed that the time scale for transition from one value to the other (referred to herein as the secondary period) was several orders of magnitude bigger than the vortex-shedding period. The duration between transitions follows a Poisson distribution and is therefore random. The average length of time between transitions decreased with an increase in velocity. This is consistent with our observation of the secondary period being one order of magnitude more than the primary period. Le Gal *et al.* (1990) argue that the Reynolds number plays an important role in determining the duration of flopping. The fundamental difference with Kim & Durbin (1988), however, is that, in the present case, flopping is observed at a relatively high gap ratio – possibly because of the larger number of cylinders, as noted earlier.

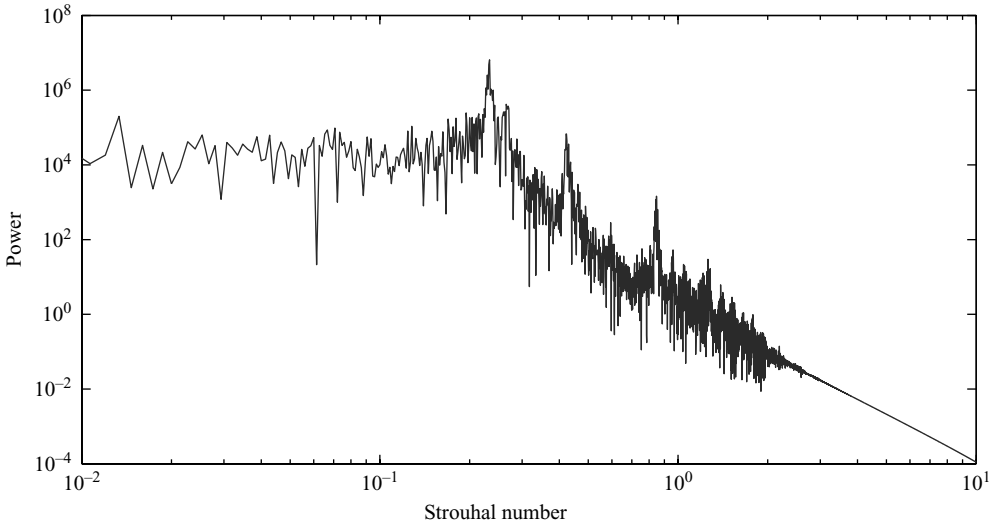

FIGURE 12. Power spectra of drag coefficient signal, for a nine-cylinder row at $s/d = 2.0$ and $Re = 80$. Power is in arbitrary units.

3.4. *Chaotic flow* ($s/d \leqslant 1.0$)

Although the vorticity contours in figure 13 appear to be qualitatively similar to that at $s/d = 2$ (figure 10*b*) in that the shedding is not synchronized, important differences exist between the two flow regimes. The small semblence that existed in the previous regime is now fully lost. Unlike the previous regime, the vortices are not apparent even immediately downstream of the cylinders, and some of the wakes appear substantially narrower or wider than normal wakes. For example in figure 13(*a*), the wake behind cylinder C_1 is narrow and that behind C_2 is wide and there is no formation of vortex behind cylinder C_2 at this instant. Note that the pattern of narrow and wide does not alternate with respect to the cylinder number. The flow in gaps for this regime is more like a jet.

These results are consistent with the experimental observation of Cheng & Moretti (1988) that some of the wakes may be very wide. Ishigai & Nishikawa (1975) noted that a vortex is formed only in the narrow wakes which also agrees with the present results. The flow behaviour is again in qualitative agreement with the experimental results of Bradshaw (1965) with circular cylinders at $Re = 1500$ and similar spacing. It was observed that the flow in the gap merges behind the cylinders and this phenomena was termed as merging of jets by Bradshaw (1965). He reported that merging of up to four jets can occur; although some evidence of this behaviour is present at $x/d \approx 1$ (figure 13*a*, *b*), it is not so apparent from the present simulations as in the experiments. Presumably, the flow Reynolds number is too small in the simulations to observe merging of jets. The streak-line photographs of Guillaume & LaRue (1999) for three cylinders showing a relatively narrow and short wake behind one of the cylinders and a relatively wide and long wake behind the other cylinders are reproduced here in figure 14 for comparison and further discussion.

The most important difference in the time series of drag coefficient for $s/d \leqslant 1$ (figure 15) with respect to that at $s/d = 2.0$, is that the secondary shedding cycles are no longer in anti-phase with respect to each other. The power spectra in figure 16 is broad with little preference for a dominant frequency. The diffused peak at a Strouhal

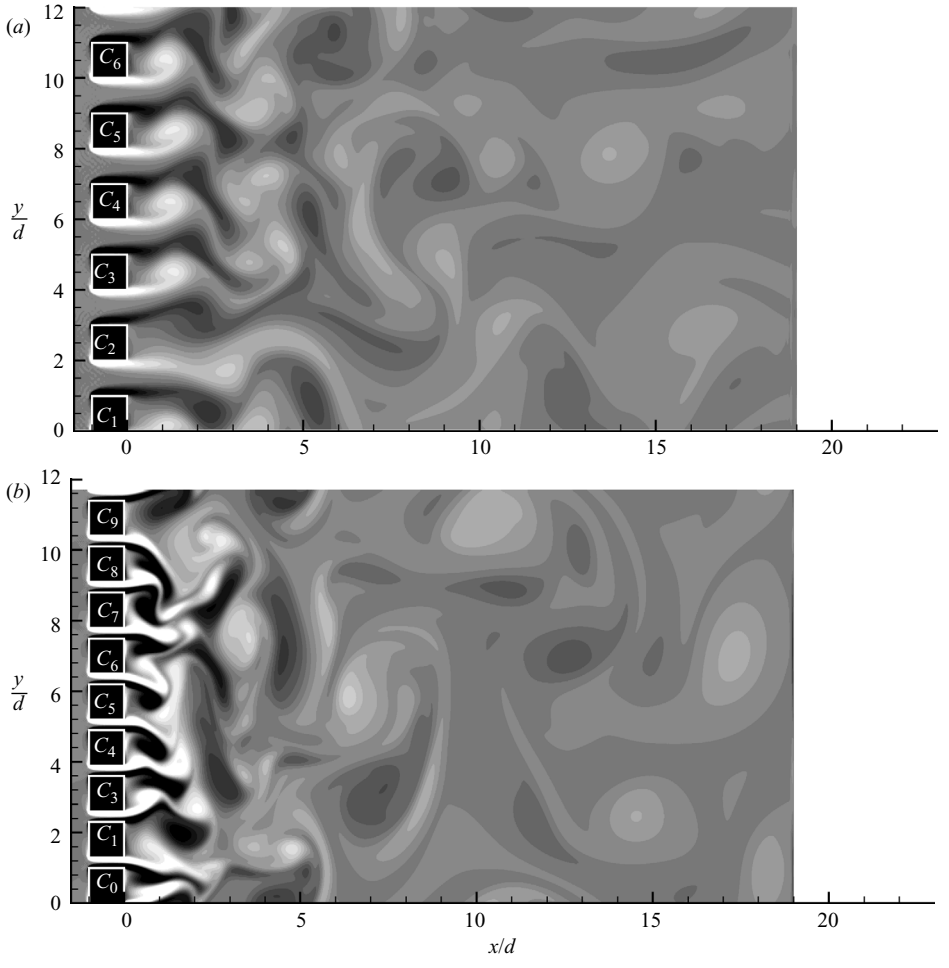

FIGURE 13. Vortex shedding from cylinders for (*a*) $s/d = 1.0$, and (*b*) $s/d = 0.30$ ($Re = 80$). The location of the cylinders is marked by a black square with a white outline.

number of 0.30 corresponds to the vortex-shedding frequency, while the peak at a Strouhal number of 0.60 is its harmonic. Note the absence of a peak corresponding to the secondary Strouhal number (in contrast to figure 12). These characteristics can be used to further differentiate the chaotic regime with respect to the quasi-periodic-II regime.

3.5. *Summary of the various regimes*

In the previous sections, definitions of various flow regimes were proposed. The demarcation of the flow regimes is based on either vorticity or signal for drag coefficient. The present simulations reveal the existence of a synchronized regime, two quasi-periodic regimes, and a chaotic regime. In the synchronized regime, the vortex shedding from any cylinder has a definite phase relationship with shedding from any other cylinder at any given instant, after initial transients have died out. The period of shedding from any cylinder is also the same for every primary (vortex-shedding) cycle in this regime. The vortex-shedding period is, however, different for consecutive cycles, even for the same cylinder in the quasi-periodic regimes. The primary cycle

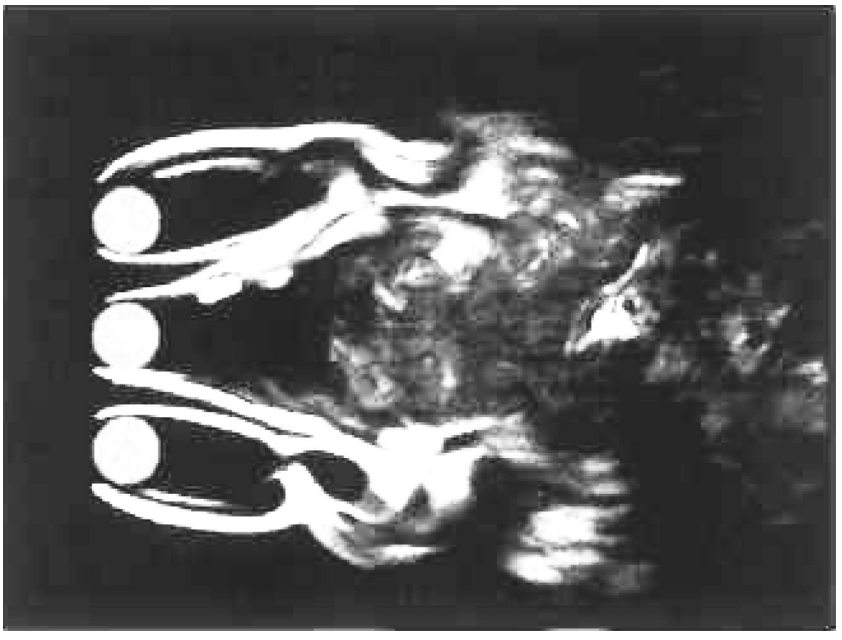

FIGURE 14. Flow visualization for three side-by-side circular-cylinders at $s/d = 0.75$ and $Re = 4400$, showing a wide wake behind the middle cylinder and narrow wakes behind the other two cylinders (Guillaume & LaRue 1999).

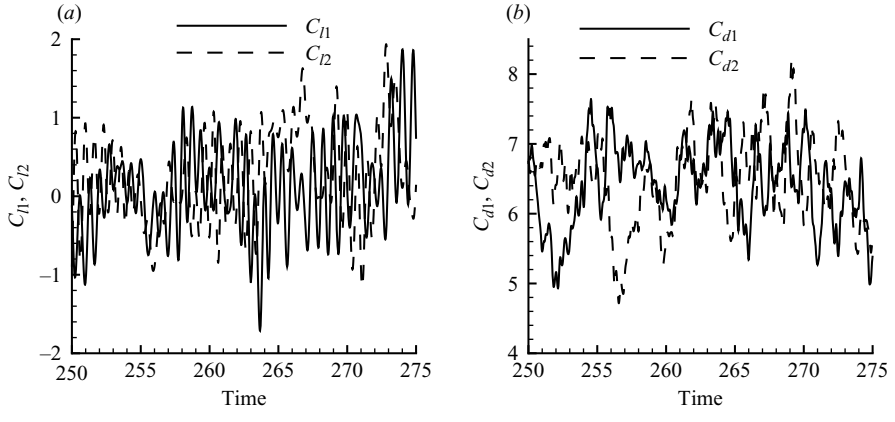

FIGURE 15. Signal of lift and drag coefficients for $s/d = 1.0$, $Re = 80$: (*a*) C_{l1}, C_{l2} versus time, and (*b*) C_{d1}, C_{d2} versus time. Note that the time on the abscissa has been normalized by the average shedding period.

can be clearly identified in the quasi-periodic-I regime, whereas the phase between secondary cycles remains constant in both the quasi-periodic regimes. The reason for the existence of the secondary cycle is discussed later. The flow in the last regime, however, does not show orderly patterns and is therefore referred to as a chaotic regime. Further justification for defining the regimes as above will be provided in § 6.2. In the following, we review the various regimes proposed in the literature – most of these studies are, however, for two circular cylinders.

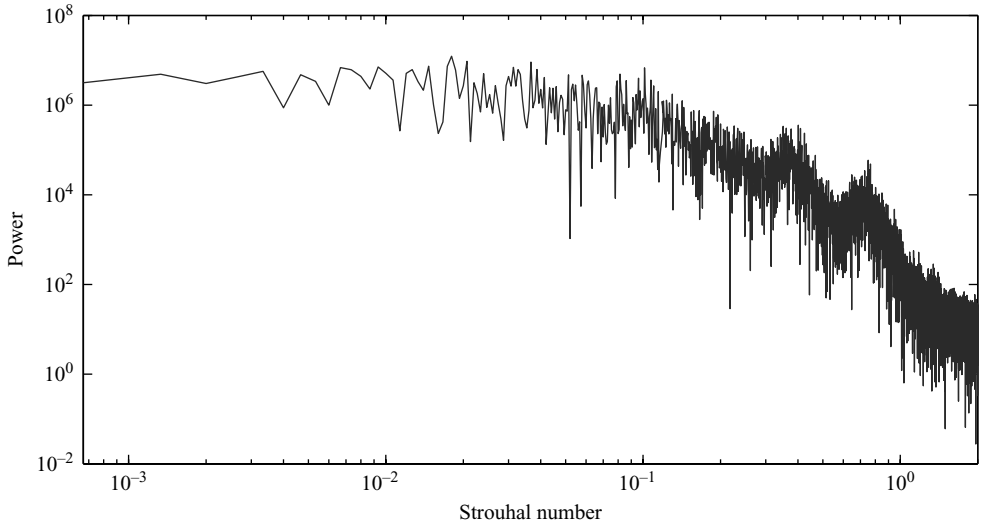

FIGURE 16. Power spectra of drag coefficient signal, for a nine-cylinder row at $s/d = 1.0$ and $Re = 80$. Power is in arbitrary units.

The vortex shedding from a single cylinder is related to the spacing between the shear layers and the thickness of the shear layer. On the other hand, a cylinder in cross-flow is sometimes modelled as an oscillator, with vortex shedding being regarded as its oscillations. The concept of an oscillator was extended by Peschard & Le Gal (1996) to two side-by-side cylinders by introducing a coupling term in the Landau model, with the amount of coupling dependent on the spacing between the cylinders and the Reynolds number. A stability analysis of the resulting equations yielded the following states: in-phase locking; asymmetric locking; quasi-periodic oscillation; and antiphase locking. Ravoux *et al.* (2003) from an analysis of the lift and drag coefficients on their numerical data for circular cylinders reported the existence of two quasi-periodic regimes in addition to periodic and chaotic regimes.

The number of regimes identified here seems consistent with that mentioned in the literature; their placement with respect to spacing is, however, different. The difference is due to one or a combination of the following factors: difference in geometry; Reynolds number; and the number of cylinders present in the flow.

4. Variation of integral parameters with spacing

The variation of flow parameters such as mean drag coefficient, shedding frequency and phase difference between vortex shedding, with respect to gap ratio have been summarized in this section. While the mean C_d and St provide information about the type of interaction in different flow regimes, the phase difference relates the positions of the vortices with respect to the cylinders and each other.

As can be seen from figure 17(a), the mean drag coefficient increases with a decrease in s/d ratio. The increase is slow up to $s/d = 4$, and picks up beyond it. The maximum drag on the cylinders for the cases investigated can be up to 20 times more than that for an isolated cylinder. It is reassuring that, for $s/d > 10.0$ the drag coefficient asymptotes to 1.638, which is within 7 % of the value of 1.533 for a single square cylinder in the free stream (Sharma & Eswaran 2004). The value seems to match that for a free-stream flow because each cylinder behaves as an isolated one at high

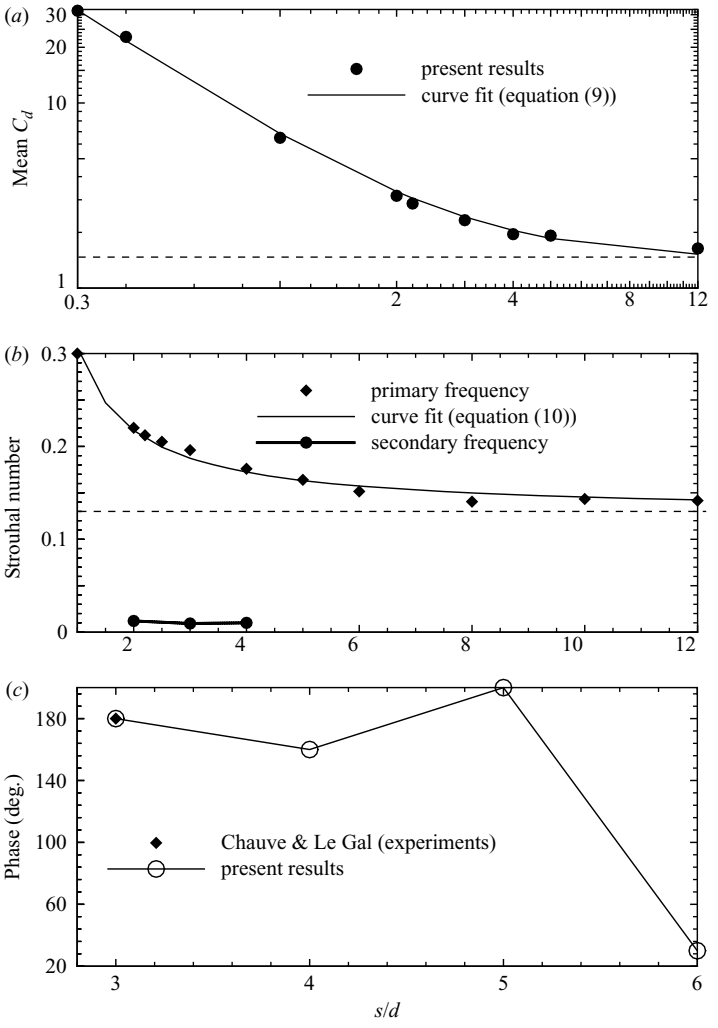

FIGURE 17. Variation of (*a*) mean C_d, (*b*) Strouhal number, and (*c*) phase difference of shedding between first and second cylinders, with spacing. Note the log–log scale in (*a*) used to bring out the trend clearly. In (*a*) and (*b*), the dashed line shows the corresponding value for flow past a single square cylinder. In (*c*), the phase lag as determined from the data of Chauve & Le Gal (1992) is also shown.

spacings. The relationship between mean C_d and s/d can be described by:

$$C_d = 1.53 - 1.30\xi + 6.60\xi^2 \quad \text{where} \quad \xi = \frac{1}{(s/d)^{0.67}}. \tag{9}$$

Equation (9) is chosen such that it gives the mean value of C_d for a single cylinder when $s/d \to \infty$. Note that (9) has the same functional form as that of mean C_d with Reynolds number (see example Khan, Culham & Yovanovich 2005), with Re replaced by s/d; the difference being that the exponent of s/d is 0.67 rather than 0.5. The above functional form is found to work better than employing a higher-order polynomial. Equation (9) has also been plotted in figure 17(*a*) and fits the computed values to within 7 %.

s/d	fd/U_0	U_{gap}/U_0	fd/U_{gap}	U_{avg}/U_0	fd/U_{avg}
2.0	0.220	1.668	0.137	1.500	0.147
2.2	0.217	1.598	0.136	1.454	0.149
2.5	0.205	1.518	0.135	1.400	0.146
3.0	0.196	1.418	0.138	1.333	0.147
4.0	0.175	1.294	0.135	1.250	0.140
5.0	0.164	1.228	0.133	1.200	0.137
6.0	0.156	1.186	0.132	1.166	0.134
8.0	0.145	1.118	0.131	1.126	0.129
10.0	0.143	1.090	0.130	1.100	0.130
12.0	0.141	1.080	0.130	1.084	0.130

TABLE 5. Variation of Strouhal number based on uniform (U_0), gap (U_{gap}) and average (U_{avg}) velocities, as a function of spacing. The gap velocity corresponds to the time-average velocity at the gap centre, obtained from the simulations. The average velocity is calculated by dividing the incoming volume flux by the open area.

The Strouhal number ($= fd/U_0$ where f is the shedding frequency of the vortices) is computed for each s/d ratio and is plotted in figure 17(b). The shedding frequency is computed as half the inverse of the time difference between two consecutive maxima in the time series of the drag coefficient; in regimes where the time series of drag coefficient does not show a pattern, the most dominant frequency is obtained by a spectral analysis of the drag signal. Figure 17(b) shows that the shedding frequency decreases with an increase in spacing, and then remains constant at $St = 0.14$ for $s/d > 6$. The relation between Strouhal number and spacing can be described by

$$St = 0.1275 + \frac{0.1792}{(s/d)}, \tag{10}$$

which has the same functional form as that of Strouhal number versus Reynolds number, proposed by Norberg (see Sohankar, Norberg & Davidson 1998) for a single cylinder. Breuer *et al.* (2000) and Norberg (see Sohankar *et al.* 1997) found $St = 0.132$, for flow past a single cylinder at a Reynolds number of 80, which compares favourably (within 4 %) with the asymptotic value obtained at large spacings. The spectral analysis reveals the presence of a secondary frequency in the flow for certain spacings. The Strouhal number based on secondary frequency is almost constant at 0.01 (figure 17b).

It is obvious that the fluid velocity in the gap between the cylinders increases with a reduction in spacing. Assuming that the detachment of vortices occurs at a fixed distance ($x/d \approx 2.0$) behind the cylinders (this seems to be justified for the first three regimes from the vorticity plots presented earlier), a larger streamwise velocity leads to a shortened time for detachment; hence, the shedding frequency increases. Upon extending the above reasoning to $s/d > 6.0$ where the period of vortex shedding remains constant, it can be argued that there is little interaction between fluid particles passing over adjacent cylinders at these higher spacings.

To check the argument about the effect of gap velocity, we compute the modified Strouhal number defined as fd/U_{gap} where U_{gap} is the time-average velocity at the gap centre. Table 5 shows that the modified Strouhal number remains approximately constant (variation of 5 %) for a large range of spacings ($2.0 \leqslant s/d \leqslant 12.0$). Further, the symptotic value is in good agreement with the value for a single cylinder. This shows that shedding is primarily affected by, and is proportional to, the average

gap velocity. Note that in the modified Strouhal number the velocity scale has been changed, but not the length scale. In fact, the Strouhal number defined as above is more instructive than the Strouhal number defined as fs/U_{gap} (which can easily be computed from data in the table) or fd/U_{avg} (table 5). However, redefining the secondary Strouhal number based on a different velocity or length scales does not reveal additional information, and is therefore not presented.

Figure 17(*c*) shows the variation in phase difference of vortex shedding between adjoining cylinders with spacing in the synchronized and the quasi-periodic-I flow regimes. The phase difference is calculated by examining the time signal for the lift coefficient from adjoining cylinders, and only spacings where shedding from adjoining cylinders is invariant with time are being reported. It can be seen from the figure that for $3.0 \leqslant s/d \leqslant 5.0$ the phase difference is close to 180° (implying that the vortex shedding is approximately in the anti-phase mode); whereas at $s/d = 6.0$ (with phase difference close to 0°) the vortex shedding is in the in-phase mode. Note that shedding is not perfectly in-phase or anti-phase, only close to them. The presence of phase lag in vortex shedding has not been reported in the literature, perhaps because of a paucity of quantitative information noted above, although it is evident from the data of Chauve & Le Gal (1992).

The mean C_d, St and flow pattern suggest different spacings when the interaction between the cylinders ceases. Based on all the observations together, we believe that when $s/d \leqslant 6.0$, the wakes behind cylinders interact whereas no significant interaction takes place at larger spacings.

5. Vorticity dynamics

As seen in § 3.1, the instantaneous vorticity field reveals interesting patterns (in-phase and anti-phase vortex shedding). In this section, we show that the continuation of the pattern generated at the downstream end of the cylinders, should be governed by the induction of velocity from the surrounding vortices on a given vortex; the same should apply to stretching of vortices in the transverse direction. The motion of vortices for the synchronized and quasi-periodic regimes are analysed using vorticity dynamics in this section.

5.1. *Synchronized and quasi-periodic-I regimes*

Consider vortex 1 in figure 5(*b*): since the time period for shedding of consecutive vortices is constant for $s/d = 5.0$ and the average convective velocity from the centre of vortex 7 to the centre of vortex 1 is almost the same; therefore, vortices 7 and 10 should be equidistant from vortex 1, as is apparent from the figure. Further, as can be seen from figure 18, the vortex strength is approximately constant for $x/d > 5$; therefore, the strength of vortices 7 and 10 should be approximately the same. Because of like signs, the induced velocity in the lateral direction computed using (7) of one vortex at the centre of vortex 1 is approximately cancelled by the other. A similar argument applies to vortex pairs 6, 9 and 5, 8, i.e. their effects on vortex 1 also cancel. In fact, based on a similar argument, it is possible to generalize and say that, if the cylinders are shedding vortices at a constant frequency, then irrespective of the phase difference in vortex shedding, the effect of surrounding vortices on a given vortex (all having the same sign) cancels out; this is apparent from the application of (7) assuming vortices of approximately equal strength.

Now examining the effect of neighbouring vortices with opposite sign to the vortex of interest: vortices 2 and 3 along with vortex 4 forms an equilateral triangle, with

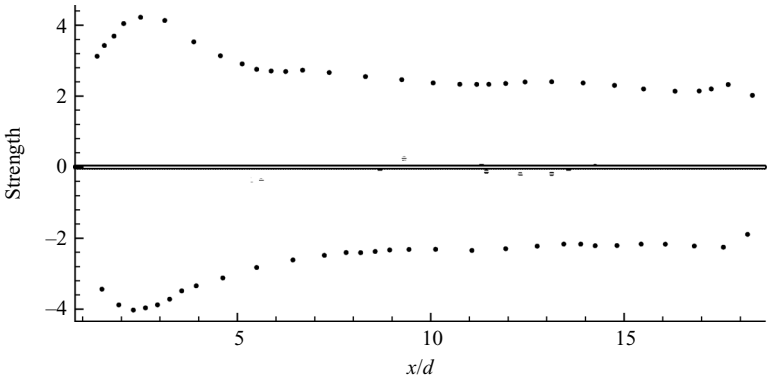

FIGURE 18. Variation in strength of vortices (in arbitrary units) with streamwise distance, at $s/d = 4.0$ and $Re = 80$.

vortex 1 as the centroid (figure 5*b*). Note that the same configuration applies for the next nearest neighbours, and so on. Therefore, again, application of (7) suggests that the effect of all surrounding vortices cancels out and each vortex moves almost parallel to the streamwise direction with little transverse movement or merging. We will see in the next section that a small transverse motion which may remain from all the cancelling effects mentioned above, is also important.

The above argument was confirmed by computing the velocity of each vortex as a result of the influence of surrounding vortices at a given instant, and then the streamwise velocity is superimposed over this induced velocity. It was further found that the average transverse velocity as well as its fluctuations are almost zero in the gap centreline region (Kumar 2006) for the entire range covered in these simulations.

Note that the same argument works with smaller spacings as well (i.e. up to the quasi-periodic-I regime). As seen in figure 17*b*, the shedding frequency increases with a reduction in spacing, which implies a smaller distance between the successive vortices. Similarly, owing to a reduction in spacing, the lateral distance between the vortices also reduces. The relative position of vortices, however, remains unaffected and the above argument applies.

5.2. *Quasi-periodic-II regime*

For the quasi-periodic-II regime, the vortices stretch in the transverse direction after shedding and merge further downstream. These combined vortices tend to develop a spread in the lateral direction with downstream distance and there is significant movement of fluid particles across the gap centreline (figure 10). This observation can be explained to some extent using the induced velocity argument discussed above (Kumar 2006).

Williamson (1985) argues that in regimes where vortices from adjoining cylinders merge, four regions can be identified when travelling downstream. In the region closest to the cylinders, two parallel in-phase streets are formed. A transitory region follows this, before the two separate wakes develop into a combined binary street. Finally, the binary vortices coalesce into a single vortex. Our simulations support the existence of all these regions for a large number of cylinders in the flow (see for example figure 10).

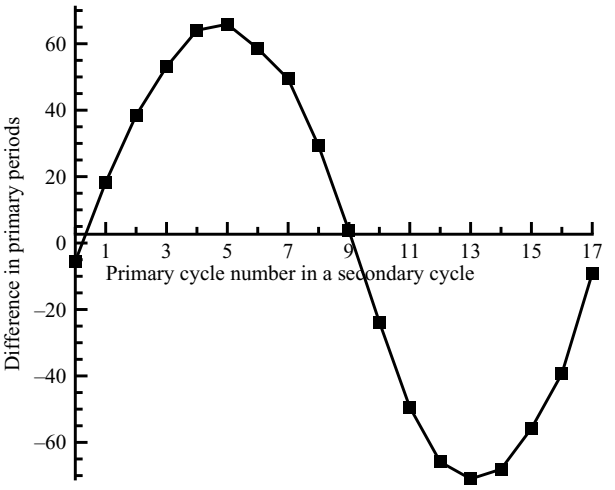

FIGURE 19. Difference in primary shedding cycle periods (iterations) of adjoining cylinders as a function of primary cycle number, over a secondary cycle ($s/d = 4.0$, $Re = 80$, 1830 time iterations correspond to a Strouhal number of 0.175). Owing to the periodic nature of the secondary cycle, this difference is plotted over one secondary cycle only. Note that the difference shows a sinusoidal variation implying that a longer primary cycle of one cylinder corresponds to a shorter primary cycle of the adjoining cylinders.

6. Secondary (cylinder interaction) frequency

In this section, we explore the origin of the secondary frequency, discuss its implication on the resulting flow, and bring about relevant observations from the literature. It is proposed that the secondary frequency is due to a relatively narrow wake behind one of the cylinders and a relatively wide wake behind the adjoining cylinders; an interchange in the order of narrow and wide wakes with time takes place, completing the cycle. The argument is first presented with respect to $s/d = 4.0$ and than generalized to other spacings.

6.1. *Origin of secondary frequency*

As is evident from table 4, a variation in primary period over a secondary cycle occurs with $s/d = 4.0$. This data along with the phase information in figure 17(c) can be used to find the primary shedding cycle periods of cylinders. Figure 19 shows the difference in primary periods of adjoining cylinders as a function of primary cycle number, over a secondary cycle. The difference is sinusoidal, implying that a longer primary cycle of one cylinder corresponds to a shorter primary cycle of the adjoining cylinders, and vice versa. This difference leads to the formation of short and long wakes, with a longer period correlating with a shorter wake. Figure 20(a) shows that a smaller longitudinal position is correlated with a smaller lateral position (called 'short and narrow' wake), and vice-versa ('long and wide' wake). This is clear upon examining the vortex pairs 1 and 5, 2 and 6, 3 and 7, and 4 and 8, which are on opposite sides with respect to their cylinder centrelines, but their longitudinal and lateral locations are different with respect to each other.

It turns out that the vortices corresponding to long wide wakes are faster moving than their short narrow wake counterparts. Therefore, as the vortices move further downstream, the vortices corresponding to long wakes move to still larger lateral positions, i.e. the long wake widens further; on the other hand, the short wake narrows further. This observation is supported by data in figure 19. This picture

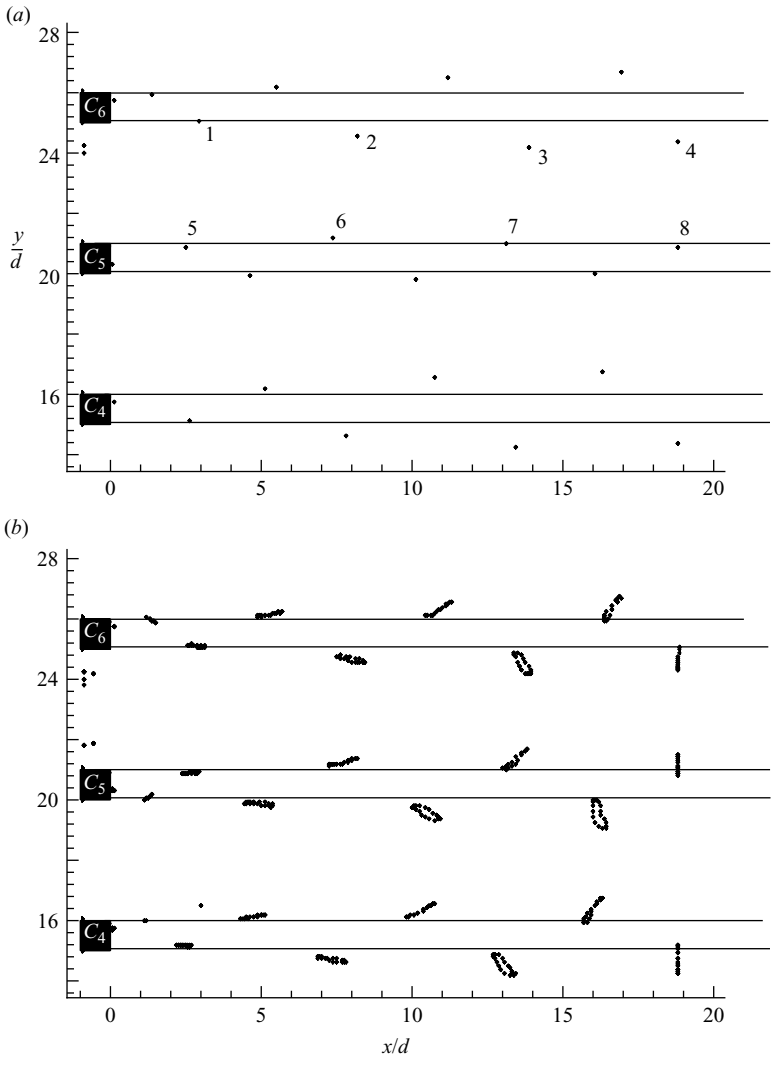

FIGURE 20. (*a*) The location of vortices centres, shed from cylinders C_4, C_5 and C_6 at $s/d = 4.0$, showing a relatively short and narrow wake behind cylinder C_5 and relatively long and wide wakes behind the other two cylinders. (*b*) The location of the centre of vortices shed from cylinders C_4, C_5 and C_6 at the end of a primary cycle, over one secondary cycle ($s/d = 4.0$, $Re = 80$). The lines parallel to cylinders top and bottom surfaces are drawn to highlight the transverse position of vortices centre as they move downstream.

applies untill further widening or narrowing is not possible, and then the wide wake starts to narrow and the narrow wake starts to widen. The secondary period corresponds to the time interval in which a narrow wake behind one cylinder becomes wide and then narrows again.

To strengthen the above argument, the positions of vortices are followed over one secondary cycle. Each curve in figure 20(*b*) comprises 18 data points representing the position of vortex centres after each vortex-shedding (primary) cycle. It is evident that the positions of vortex centres do not coincide, as they should if only one (primary) cycle were present; rather, they form closed loops, highlighting the presence of another

(secondary) frequency. In particular, just behind the cylinders ($x/d \leqslant 5$), the wakes primarily transit between short and long wakes, because the vortex positions scan a straight line parallel to the streamwise direction. Subsequently, the vortex positions scan a line at an angle with respect to the streamwise coordinate, representing both long wide and short narrow wakes. These observations are in accord with the above argument of long (short) wakes (because of variation in the primary cycle) leading to long wide (short narrow) wakes and the appearance of a secondary cycle.

Further credence to the proposition on the origin of the secondary frequency is obtained by examining both vorticity and pressure fields at the same instant. A long wake behind a cylinder corresponds to a relatively high pressure downstream of that cylinder. As the pressure force is the major constituent of the overall drag force (about 90 % at this Reynolds number and spacing), the drag coefficient is small in the case of a long wake. Conversely, a short wake downstream of a cylinder corresponds to a lower downstream pressure, and a larger drag force. As already discussed, the secondary signals from adjacent cylinders are in anti-phase (figure 8*b*), which means that whenever a narrow wake is formed behind one cylinder, a wide wake is formed behind its two neighbours, and vice versa, leading to alternatively high and low values of the drag coefficient. Note that Guillaume & LaRue (1999) also observed anti-phase flopping for three side-by-side circular cylinders (figure 14).

6.2. *Discussion on secondary frequency*

Three points on secondary frequency are worth noting. First, the secondary frequency makes an increasingly dominant contribution to the C_d signal with a reduction in spacing. For example, at $s/d = 5.0$, there is no apparent component of secondary frequency in the drag coefficient; the amplitude of the drag coefficient (of approximately 0.03) is brought about by the primary (vortex shedding) cycle. (For comparison, the amplitude of C_d for a single cylinder is about 0.01 with a mean of 1.533.) At $s/d = 4.0$ and 3.0, the drag coefficient varies by 0.33 and 0.64, respectively, i.e. about 11 and 21 times the primary shedding amplitude at large spacings. A further increase in the amplitude of drag coefficient to 0.80 and 0.96 at $s/d = 2.2$ and 2.0 is also due to the secondary frequency. Owing to correlation and proportionality between the secondary frequency and cylinder spacing, we propose that the secondary frequency is a new component brought about by the interaction of the wakes. The secondary frequency can therefore also be regarded as cylinder interaction frequency.

Secondly, the secondary frequency affects even the primary frequency, as seen by the variation in primary cycle over one secondary cycle. That is, although it is argued in § 6.1 that variations in the primary cycle lead to a secondary cycle, the cause-and-effect cannot really be determined. As noted in table 4, the cycle-to-cycle variation in period increases with a decrease in spacing (4 % at $s/d = 4.0$ and 10 % at $s/d = 3.0$); also the number of primary cycles encompassed in a secondary cycle increases with spacing (from 17 cycles at $s/d = 4.0$ to 21 cycles at $s/d = 3.0$). Extending it further, we believe that at smaller spacings the cycle-to-cycle variation in period becomes so large that the primary cycle itself loses meaning (the minimum fluctuations in C_d at $s/d = 4.0$, 2.2 and 2.0 are approximately 0.04, 0.02 and 0.01, respectively). That is, the shedding of vortices becomes irregular, leading to a choatic regime, as observed for $s/d \leqslant 1.0$ in these computations. All the regimes can therefore be construed as an interplay between the two (primary and secondary) cycles: only the primary cycle is important in the synchronized regime (figure 6). When both are of comparable magnitude, the two frequencies lead to quasi-periodic regimes. Further, in the quasi-periodic-I regime, the primary cycle is stronger than the secondary (figure 8) whereas

the secondary dominates in the quasi-periodic-II regime (figure 11). Finally, when the secondary frequency overwhelms the primary, a chaotic regime results (figure 15).

Thirdly, we believe that the connection between wake lengths and frequencies in the flow has not been clearly elucidated in the literature. The interaction of the two frequencies, as proposed here, can act as a unifying agent for the various (sometimes contradictory) results in the literature.

7. Conclusions

A numerical study of flow around a row of square cylinders placed side-by-side has been carried out using the two-dimensional lattice-Boltzmann method at different separation ratios ($s/d = 0.3$–12) and a Reynolds number of 80. The focus has been to understand the flow physics as revealed by these detailed computations. Based on the variation of mean drag coefficient and shedding period with respect to spacing, it is concluded that when $s/d \leqslant 6.0$, the wakes behind cylinders interact, resulting in a variety of flow patterns. At larger spacings, no significant interaction between the wakes is observed. The mean drag coefficient and shedding frequency are about 7 % higher than for an isolated cylinder at larger spacings, but becomes drastically more with a reduction in spacing. The variation of shedding period with respect to gap ratios also reveals that shedding is primarily affected by, and is proportional to, the average gap velocity for $2.0 \leqslant s/d \leqslant 12.0$.

It is found that synchronized vortex shedding takes place for $s/d \geqslant 5.0$, whereby vortices shed from any cylinder are at constant frequency and have a definite phase relationship with vortices shedding from other cylinders. Consequently, there is only one frequency in the time signal corresponding to the shedding cycle, and no transverse movement of vortices takes place. For $3.0 \leqslant s/d \leqslant 4.0$, shedding from one cylinder shows a definite phase relationship with shedding from other cylinders, but the shedding period is not constant; the time signal for this regime also shows a second frequency. The time period corresponding to secondary frequency is an order of magnitude larger than the vortex-shedding period; the secondary frequency is believed to correspond to narrow and wide wakes. It is shown that the secondary frequency makes a dominating contribution to C_d and its contribution increases with a decrease in spacing (about 11 and 21 times compared to large spacings for $s/d = 4.0$ and 3.0, respectively). Relatively low shedding period and large drag coefficient corresponds to a short wake and higher periods, and small drag coefficient corresponds to long wake. Consecutive cylinders are in anti-phase with respect to the secondary frequency.

Another quasi-periodic regime occurs for $1.0 < s/d < 3.0$ where there is no definite pattern of vortex shedding from a cylinder as well as between shedding from adjacent cylinders. A secondary cycle can be identified in this regime also from a pronounced effect on drag force, so much that the effect of shedding frequency on drag coefficient becomes negligibly small at smaller s/d and fluctuations observed are mainly due to the secondary frequency. At $s/d \leqslant 1.0$, there is no semblence in the flow. It is argued that the different flow regimes can be explained based on interaction between vortex shedding and cylinder interaction frequencies. Some essential features of the various regimes have been summarized in table 6.

The flow patterns observed in the different flow regimes have been explained on the basis of vorticity interaction. For $s/d \geqslant 3.0$, the vortices are distinct and clearly apparent without significant lateral spread. There is not much movement of fluid across the gap centreline. At $s/d \leqslant 2.2$, the vortices stretch in the transverse direction after shedding and merge further downstream to form a single vortex. There is

Spacing	Observation	Regime
$s/d \geqslant 8$	No significant interaction	
$s/d = 6$	Interaction manifests with cylinders shedding vortices in-phase with a phase lag	Synchronized
$s/d = 5$	Phase lag increases to about 180° leading to a transition from in-phase to anti-phase shedding	Synchronized
$s/d = 4$	Secondary frequency appears due to a lateral movement of vortices (cancellation of induced velocity from the surrounding vortices is no longer perfect)	Quasi-periodic-I
$s/d = 3$ (and below)	Substantial lateral movement of vortices	Quasi-periodic-II
$s/d < 1$	Secondary frequency overwhelms the primary frequency; no clear peak in the spectrum unlike above regimes	Chaotic regime

TABLE 6. Summary of the various flow regimes at $Re = 80$. Note that the regime boundaries are not well resolved, and therefore the spacing demarcating the different regimes is only approximate.

significant movement of fluid particles across the gap centreline at lower spacings. These results are expected to be important both fundamentally and for some of the applications identified above.

We are grateful to Mr C. M. Sewatkar for the computations in § 2.5 and for independently verifying some of the results presented herein. The financial support of the Department of Science and Technology, New Delhi is acknowledged.

REFERENCES

AGRAWAL, A. & AGRAWAL, A. 2006 Three-dimensional simulation of gaseous slip flow in different aspect ratio microducts. *Phys. Fluids* **18**, 103604.

AGRAWAL, A., DJENIDI, L. & ANTONIA, R. A. 2006 Investigation of flow around of a pair of side-by-side square cylinders using the lattice Boltzmann method. *Comput. Fluids* **35**, 1093–1107.

BEARMAN, P. W. & WADCOCK, A. J. 1973 The interaction between a pair of circular cylinders normal to a stream. *J. Fluid Mech.* **61**, 499–511.

BRADSHAW, P. 1965 The effect of wind-tunnel screens on nominally two-dimensional boundary layers. *J. Fluid Mech.* **22**, 679–687.

BREUER, M., BERNSDORF, J., ZEISER, T. & DURST, F. 2000 Accurate computations of the laminar flow past a square cylinder based on two different methods: lattice-Boltzmann and finite-volume. *Intl J. Heat Fluid Flow* **21**, 186–196.

BURATTINI, P., LAVOIE, P., AGRAWAL, A., DJENIDI, L. & ANTONIA, R. A. 2006 Power law of decaying homogeneous isotropic turbulence at low Reynolds number. *Phys. Rev.* E **73**, 066304.

CHAUVE, M. P. & LE GAL, P. 1992 Complex bi-orthogonal decomposition of a chain of complex wakes. *Physica* D **58**, 407–413.

CHEN, S. & DOOLEN, G. 1998 Lattice Boltzmann method for fluid flows. *Annu. Rev. Fluid Mech.* **30**, 329–364.

CHENG, M. & MORETTI, P. M. 1988 Experimental study of the flow field downstream of a single tube row. *Expl Thermal Fluid Sci.* **1**, 69–74.

FARRANT, T., TAN, M. & PRICE, W. G. 2001 A cell boundary element method applied to laminar vortex shedding from circular cylinders. *Computers Fluids* **30**, 211–236.

FRANKE, R., RODI, W. & SCHONUGH, B. 1990 Numerical Calculation of Laminar Vortex-Shedding Flow Past Cylinders. *J. Wind Engng Indust. Aerodyn.* **35**, 237–257.

FRISCH, U., HASSLACHER, B. & POMEAU, Y. 1986 Lattice gas automata for the Navier-Stokes equations. *Phys. Rev. Lett.* **56**, 1505–1508.

Guillaume, D. W. & LaRue, J. C. 1999 Investigation of the flopping regime with two-, three- and four-cylinder arrays. *Exps. Fluids* **27**, 145–156.

Ishigai, S. & Nishikawa, E. 1975 Experimental study of structure of gas flow in tube banks with tube axes normal to flow. Part II: On the structure of gas flow in single-column, single-row, and double-rows tube banks. *Bull. JSME* **18**, 528–535.

Kang, S. 2003 Characteristics of flow over two circular cylinders in a side-by-side arrangement at low Reynolds numbers. *Phys. Fluids* **15**, 2486–2498.

Khan, W. A., Culham, J. R. & Yovanovich, M. M. 2005 Fluid flow around and heat transfer from an infinite circular cylinder. *J. Heat Transfer* **127**, 785–790.

Kim, H. J. & Durbin, P. A. 1988 Investigation of the flow between a pair of circular cylinders in the flopping regime. *J. Fluid Mech.* **196**, 431–448.

Kobayashi, T. 1984 In *Shashinshu Nagare* (Photograph Album of Flows), p. 43. Japan Society of Mechanical Engineers, Maruzen Tokyo.

Kolar, V., Lyn, D.A. & Rodi, W. 1997 Ensemble-averaged measurements in the turbulent near wake of two side-by-side square cylinders. *J. Fluid Mech.* **346**, 201–237.

Kumar, S. R. 2006 Low Reynolds number flow around row of square cylinders. M.Tech. thesis, Department of Mechanical Engineering, Indian Institute of Technology, Bombay.

Kundu, P. K. 1990 *Fluid Mechanics*. Academic Press, San Diego, CA, USA.

Le Gal, P., Chauve, M. P., Lima, R. & Rezende, J. 1990 Coupled wakes behind two circular cylinders. *Phys. Rev.* A **41**, 4566–4569.

Le Gal, P., Peschard, I., Chauve, M. P. & Takeda, Y. 1996 Collective behavior of wakes downstream a row of cylinders. *Phys. Fluids* **8**, 2097–2106.

Meneghini, J. R., Saltara, F., Siqueira, C. L. R. & Ferrari, J. A. 2001 Numerical simulation of flow interference between two circular cylinders in tandem and side-by-side arrangements. *J. Fluids Struct.* **15**, 327–350.

Mizushima, J. & Akinaga, T. 2003 Vortex shedding from a row of square bars. *Fluid Dyn. Res.* **32**, 179–191.

Mizushima, J. & Takemoto, Y. 1996 Stability of the flow past a row of square bars. *J. Phys. Soc. Japan* **65**, 1673–1685.

Peschard, I. & Le Gal, P. 1996 Coupled wakes of cylinders. *Phys. Rev. Lett.* **15**, 3122–3125.

Ravoux, J. F., Nadim, A. & Haj-Hariri, H. 2003 An embedding method for bluff-body flows: interactions of two side-by-side cylinder wakes. *Theor. Comput. Fluid Dyn.* **16**, 433–466.

Robichaux, J., Balachandar, S. & Vanka, S. P. 1999 Two-dimensional floquet instability of the wake of square cylinder. *Phys. Fluids* **11**, 560–578.

Saha, A. K., Biswas, G. & Muralidhar, K. 2003 Three-dimensional study of flow past a square cylinder at low Reynolds numbers. *Intl J. Heat Fluid Flow* **24**, 54–66.

Saha, A. K., Muralidhar, K. & Biswas, G. 2000 Vortex structures and kinetic energy budget in two-dimensional flow past a square cylinder. *Comput. Fluids* **29**, 669–694.

Sharma, A. & Eswaran, V. 2004 Heat and Fluid Flow across a Square Cylinder in the Two-Dimensional Laminar Flow Regime. *Numer. Heat Transfer* A **45**, 247–269.

Slaouti, A. & Stansby, P. K. 1992 Flow around two circular cylinders by the random vortex method. *J. Fluids Struct.* **6**, 641–670.

Sohankar, A., Norberg, C. & Davidson, L. 1997 Numerical simulation of unsteady low-Reynolds number flow around rectangular cylinders at incidence. *J. Wind Engng Ind. Aerodyn.* **69–71**, 189–201.

Sohankar, A., Norberg, C. & Davidson, L. 1998 Low-Reynolds number flow around a square cylinder at incidence: study of blockage, onset of vortex shedding and outlet boundary condition. *Intl J. Numer. Meth. Fluids* **26**, 39–56.

Succi, S. 2001 *Lattice Boltzmann Method for Fluid Dynamics and Beyond*. Oxford University Press.

Sumner, D., Wong, S. S .T., Price, S. J. & Paidoussis, M. D. 1999 Fluid behaviour of side-by-side circular cylinders in steady cross-flow. *J. Fluids Struct.* **13**, 309–338.

Valencia, A. & Cid, M. 2002 Turbulent unsteady flow and heat transfer in channels with periodically mounted square bars. *Intl J. Heat Mass Transfer* **45**, 1661–1673.

Williamson, C. H. K. 1985 Evolution of a single wake behind a pair of bluff bodies. *J. Fluid Mech.* **159**, 1–18.

Zhou, Y., So, R. M. C., Liu, M. H. & Zhang, H. J. 2000 Complex turbulent wakes generated by two and three side-by-side cylinders. *Intl J. Heat Fluid Flow* **21**, 125–133.